



TiO₂ mesocrystal with exposed (001) facets and CdS quantum dots as an active visible photocatalyst for selective oxidation reactions



Xinru Li^a, Jinguo Wang^{b,*}, Yong Men^b, Zhenfeng Bian^{c,*}

^a Department of Chemical and Biomolecular Engineering, University of California, Los Angeles, CA 90095, USA

^b College of Chemistry and Chemical Engineering, Shanghai University of Engineering Science, Shanghai 201620, China

^c The Education Ministry Key Lab of Resource Chemistry, Shanghai Normal University, Shanghai 200234, China

ARTICLE INFO

Article history:

Received 25 October 2015

Received in revised form 10 January 2016

Accepted 13 January 2016

Available online 15 January 2016

Keywords:

TiO₂ mesocrystals

Exposed (001) facets

CdS quantum dots

Visible photoactivity

Selective oxidation reactions

ABSTRACT

CdS quantum dots decorated TiO₂ mesocrystals with exposed (001) facets were synthesized by solvothermal alcoholysis and subsequent ion-exchange. The as-prepared photocatalyst exhibited high activity and selectivity in selective oxidations of various alcohols to their corresponding aldehydes under visible light irradiation. The high photocatalytic efficiency could be ascribed to the CdS quantum dots with enhanced photosensitizing effect and CdS–TiO₂ heterojunction, the mesoporous structure with high surface area, and the exposed (001) facets with high surface energy and large number of oxygen vacancies, which promoted the light-harvesting, photocatalyst activation by visible lights, photoelectron-hole separation, reactant molecule adsorption and activation. Moreover, it also showed strong durability owing to the excellent stability against structural collapse and either CdS leaching or CdS corrosion.

© 2016 Elsevier B.V. All rights reserved.

1. Introduction

Mesocrystals refer to the single-crystals with mesoporous structure, which show good potential applications in various areas owing to the advantages of both the well-defined crystallization and the high surface area [1–4]. Among all the flourishing emergence of mesocrystals, TiO₂ mesocrystals have received increasing attention in photocatalytic degradation of organic pollutants, antibacterial, reduction of heavy metal ions, H₂ production via water splitting and even selective oxidation reactions [5–10]. Meanwhile, both theoretical prediction and experimental results indicate that (001) facets of anatase TiO₂ are much more reactive than other thermodynamically stable facets [9–16]. Accordingly, anatase TiO₂ mesocrystals with exposed (001) facets are expected to be the most active photocatalysts. Moreover, modification of anatase TiO₂ mesocrystals with photosensitizers may achieve visible photocatalysis, obviously which is more preferable in practical applications owing to the enhanced light-harvesting ability under sunlight irradiation. Among various photosensitizers, CdS with narrow energy band gap (2.4 eV) is most frequently employed owing to its easy modification onto TiO₂ with strong interaction and high photosensitizing efficiency [17–20]. Herein, we reported for the first time a novel TiO₂ mesocrystals with exposed (001) facets prepared

by a facile solvothermal alcoholysis, followed by modifying with CdS quantum dots through a simple ion-exchange treatment. The combination of the mesoporous structure, well-defined anatase TiO₂ crystal with exposed (001) facets and CdS photosensitizing effect resulted in high photocatalytic activity for selective oxidation of alcohols to aldehydes under visible light irradiation.

2. Experimental

2.1. Sample preparation

The TiO₂ mesocrystals with exposed (001) facets were synthesized by solvothermal alcoholysis of TiOSO₄. In a typical run of synthesis, 2.0 mL TiOSO₄ was slowly added into 40 mL *tert*-butyl alcohol and stirred for 0.5 h. Then, the mixture was transferred into a 50 mL Teflon-lined autoclave at 110 °C for 48 h. After being cooled to room temperature, the solid product was filtered and washed thoroughly with ethanol, and finally dried at 100 °C for 8.0 h. The polycrystalline TiO₂ was obtained by a traditional sol-gel route [21]. The TiO₂ mesocrystals modified with CdS (CdS/TiO₂) were prepared by ion-exchange method (see Fig. S1). Briefly, 1.0 g TiO₂ mesocrystals and a certain amount of Cd(NO₃)₂ were added into 20 mL absolute ethanol, followed by stirring for 1.0 h and ultrasound for 2.0 h, and then dried at 80 °C for 10 h. After being calcinated at 400 °C for 4.0 h to get the CdO/TiO₂ composite, it was dispersed in 100 mL 0.20 M Na₂S aqueous solution with stirring at 25 °C for 4.0 h, followed by filtering, washing with water and drying at 80 °C

* Corresponding authors.

E-mail addresses: jinguowang1982@163.com (J. Wang), bianzhenfeng@shnu.edu.cn, bianzhenfeng@163.com (Z. Bian).

Table 1
Physical structural parameters and the photocatalytic performances of different samples.

Sample	CdS loading (wt%)	S_{BET} (m^2/g)	D_p (nm)	V_p (cm^3/g)	Crystal size ^a (nm)	Conversion (%)
CST0	0	126	5.1	0.19	12	3.0
CST1	0.85	130	4.2	0.17	12	35
CST2	2.1	140	3.9	0.16	11	60
CST3	3.5	144	3.6	0.14	10	98
CST4	4.4	129	3.3	0.13	10	85
CST5	4.9	115	3.2	0.12	10	79
CSTD	3.4	110	3.6	0.13	12	72
CSTM	3.5	117	4.9	0.18	12	59
CSTP	3.5	125	7.9	0.28	11	64
CST3 ^b	3.2	138	3.5	0.14	10	89
CSTD ^b	0.82	106	3.7	0.19	12	27
CSTM ^b	0.75	115	5.1	0.19	12	15
CSTP ^b	2.9	126	7.9	0.28	11	56

^a Calculated by the Scherrer's equation based on the (1 0 1) peak of the anatase TiO_2 .

^b After being used repetitively for 4 times.

for 8.0 h. The as-received samples were denoted as CSTX, where X corresponded to different CdS loadings. The modification of polycrystalline TiO_2 with 3.5 wt% CdS quantum dots was performed in the same process and denoted as CSTP. For comparison, the TiO_2 mesocrystals with exposed (001) facets and 3.5 wt% CdS was also prepared by directly depositing TiO_2 with CdS nanoparticles obtained from the reaction between $\text{Cd}(\text{NO}_3)_2$ and Na_2S in aqueous solution containing TiO_2 mesocrystals, and denoted as CSTD. Meanwhile, the TiO_2 mesocrystals with exposed (001) facets were also manually mixed with the CdS nanoparticles previously prepared from the direct reaction between $\text{Cd}(\text{NO}_3)_2$ and Na_2S in aqueous solution, which was denoted as CSTM.

2.2. Characterization

The CdS loading was determined by inductive coupled plasma emission spectrometer (ICP, Varian, VISTAMPXICP). Structure and morphology were characterized by high-resolution transmission electron microscopy (HRTEM, JEOL JEM-2100) and X-ray diffraction (XRD, Rigaku D/Max-2000, monochromatic $\text{CuK}\alpha$ radiation). N_2 adsorption-desorption isotherms were determined on Quantachrome NOVA 4000 at 77 K, from which, surface area (S_{BET}), pore volume (V_p) and pore diameter (D_p) were calculated by applying Brunauer-Emmett-Teller (BET) and Barrett-Joyner-Halenda (BJH) models on the desorption branches. The surface electronic states were analyzed by X-ray photoelectron spectroscopy (XPS, PerkinElmer PHI 5000). All the binding energy values were calibrated by using $\text{C}_{1s} = 284.6 \text{ eV}$ as the reference. Raman spectra, photoluminescence spectroscopy (PLS) and UV–vis diffuse reflectance spectra (UV–vis DRS) were collected on a Dilor Super LabRam Π , Varian Cary-Eclipse 500 and MC-2530, respectively. The photoelectrochemical measurements were performed in a home-made three electrode quartz cell containing 0.20 M Na_2SO_4 aqueous solution under visible light irradiation ($\lambda \geq 420 \text{ nm}$), with a PAR VMP3 Multipotentiostat apparatus and a BAS Epsilon workstation. A Pt plate and a Ag/AgCl electrode were used as the counter and reference electrodes, respectively, while the work electrode was prepared by depositing 10 mg photocatalyst onto fluoride-tin oxide (FTO) conductor glass. The radical species were detected by electron spin resonance (ESR) spectrometry on a Bruker EPR A300 instrument with a 300W Xe arc lamp under visible light irradiation ($\lambda \geq 420 \text{ nm}$).

2.3. Activity test

The photocatalytic selective oxidation reaction was carried out at 25°C in a self-designed 100 mL reactor containing 50 mg photocatalysts, 10 mL benzonitrile and 0.20 mmol benzyl alcohol or

its derivatives. After reaching adsorption-desorption equilibrium in dark, the reaction was initiated by irradiating with a 300W Xe arc lamp at 15 cm away from the solution, in which all the UV lights with wavelength shorter than 420 nm were cut off by a glass filter (JB-420 nm). After reaction for 3.0 h, the reaction products were identified by a GC–MS (Agilent 6890N/5973I) and quantitatively analyzed by GC (Shimadzu, GC-17A). Blank experiments demonstrated that no significant oxidations occurred in the absence of either light irradiation or photocatalyst. The capturing experiment of active species was also conducted by the same method except addition of different scavengers with amount of 30 mmol. The reproducibility of all the activity tests was checked by repeating each result at least three times and found to be within acceptable limits ($\pm 3.0\%$).

3. Results and discussion

3.1. Structural characteristics

Table 1 shows the amount of CdS loading determined by ICP analysis. As shown in Fig. 1, the HRTEM images demonstrated that all the CSTX samples were present in well-defined anatase TiO_2 single crystal and the attached SAED images displayed the exposed (001) facets. The CdS nanoparticles homogeneously dispersed on the outer and internal channel surface of TiO_2 and the particle size kept around 2.0 nm with the increase of CdS loading up to 3.5 wt%. However, further increase in the CdS loading resulted in a rapid aggregation of CdS nanoparticles, leading to an abrupt increase of particle size to 6.0 nm. The TEM and SAED images (Fig. S2) revealed that the CSTP was present in polycrystalline anatase with dominant (101) facets and the CdS quantum dots with particle size around 2.0 nm were also uniformly deposited onto the TiO_2 outer surface. Although both CSTD and CSTM were present in well-defined anatase TiO_2 single crystal with exposed (001) facets, they contained much bigger CdS nanoparticles with the average size around 8.0 nm and 25 nm deposited onto the TiO_2 outer surface, obviously due to the different preparation methods.

The XRD patterns in Fig. 2 demonstrates that all the CSTX samples together with CSTD and CSTM were present in well-defined anatase TiO_2 crystal with the diffractive peaks around 2θ of 25.3° , 37.8° and 48° corresponding to (1 0 1), (0 0 4) and (2 0 0) facets (JCPDS 21-1272) [9,10]. The CSTX samples with CdS loading higher than 3.5 wt% displayed the well-resolved diffraction peaks around 2θ of 44° indicative of the (2 2 0) facet in cubic CdS phase (JCPDS 10-0454). However, no significant diffraction peaks indicative of CdS were observed in CSTX samples with CdS loading below 3.5 wt%, obviously due to the ultrasmall CdS particles. From CST4, CST5, CSTD to CSTM, the intensity of the diffractive peaks corre-

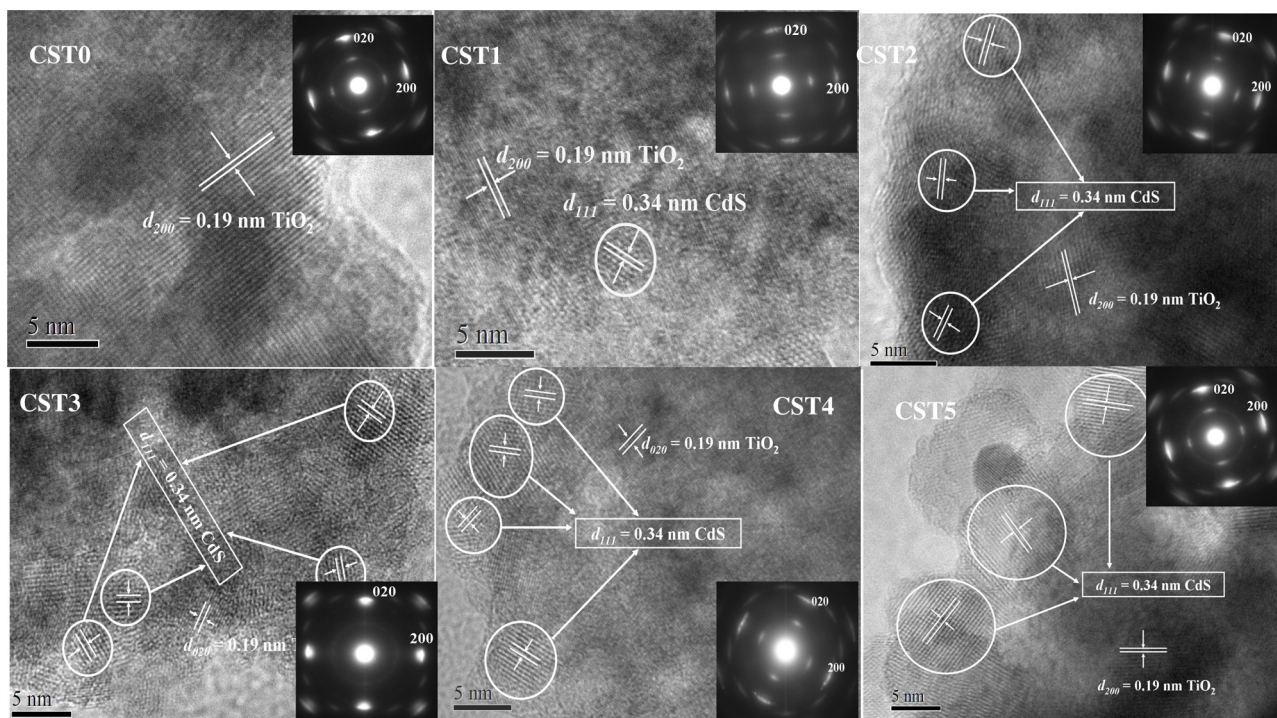


Fig. 1. The HRTEM and SAED (inset) images of different samples.

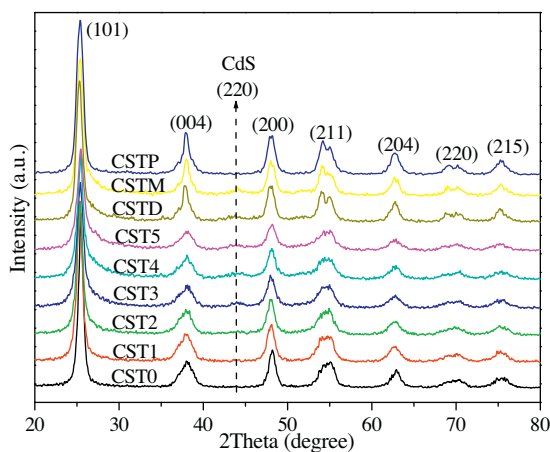


Fig. 2. XRD patterns of different samples.

sponding to CdS increased rapidly, corresponding to the increase of CdS particle size which was consistent with the aforementioned HRTEM characterizations. In comparison with pure TiO₂ mesocrystal (CST0), no significant shift of principal peaks of TiO₂ occurred in all the CdS modified TiO₂ samples (CSTX, CSTP, CSTD, CSTM), suggesting that the CdS was present in a separated phase rather than incorporated into TiO₂ lattice due to the bigger size of Cd²⁺ (97 pm) than Ti⁴⁺ (61 pm) [20]. In addition, comparison of the intensities between the XRD peaks indicative of (1 0 1) and (0 0 4) facets demonstrated that all the CSTX, CSTD and CSTM samples displayed dominant (001) facets while the CSTP showed the dominant (1 0 1) facets. From the principal XRD peaks, the TiO₂ crystal size was calculated based on Scherrer's equation. As shown in Table 1, the TiO₂ crystal size in CSTX samples decreased slightly with the increase of CdS loading while no significant change was observed in either CSTD or CSTM, suggesting that the presence of Cd²⁺ might retard the crystal growth of TiO₂.

Fig. 3 demonstrates that all the CSTX samples displayed the typical type IV N₂ adsorption-desorption isotherms with H1 hysteresis loops indicative of the mesoporous structure with relatively narrow pore diameter range [9,10,22]. Similar results were also observed in CSTP, CSTD and CSTM samples (see Fig. S3). The pore diameter decreased with the increase of the CdS loading due to the occupation of CdS particles in the mesopores. Based on the N₂ adsorption-desorption isotherms, the S_{BET}, V_p, and D_p have been calculated by using BET and BJH models, respectively. As shown in Table 1, both the V_p and the D_p decreased with the increase of CdS loading in the CSTX samples due to the occupation of CdS nanoparticles in the mesopores. The S_{BET} firstly increased with the increase of CdS loading up to 3.5 wt% owing to the decrease of TiO₂ crystal size. Further increase of the CdS loading resulted in the decreased S_{BET} due to the enhanced pore blockage by CdS nanoparticles and the unchanged TiO₂ crystal size.

The XPS spectra in Fig. 4 reveals that the Cd species in all the CST3, CSTP, CSTD and CSTM samples displayed the binding energy around 404.9 eV and 411.7 eV in Cd_{3d5/2} and Cd_{3d3/2} levels, while S showed the binding energy around 161.9 eV in S_{2p} level, corresponding to the presence of CdS [17–20]. Comparing those observed in the pure CdS, both Cd and S binding energies exhibited positive shift was observed in CST3 and CSTP indicative of the strong interaction between CdS and TiO₂ in which partial electrons transferred from CdS to TiO₂ [23]. The failure in observing binding energy shift of either Ti or O atom (see Fig. S4) could be ascribed to the extremely excess of TiO₂ in comparison with that of CdS. No significant binding energy shift of CdS was found in CSTD and CSTM due to the weak interaction between CdS and TiO₂. Obviously, CST3 and CSTP contained more CdS–TiO₂ heterojunctions than either CSTD or CSTM owing to the smaller CdS particles with enhanced number of CdS particles and especially, the strong CdS–TiO₂ interaction [24–26].

As shown in Fig. 5, the Raman spectra revealed that CST3 and CSTP displayed the peaks at 144 cm^{−1} (E_g), 394 cm^{−1} (B_{1g}), 514 cm^{−1} (A_{1g}), 636 cm^{−1} (E_g), characteristic of the anatase TiO₂ phase. The attached magnified Raman spectra from 100 to 200 cm^{−1}

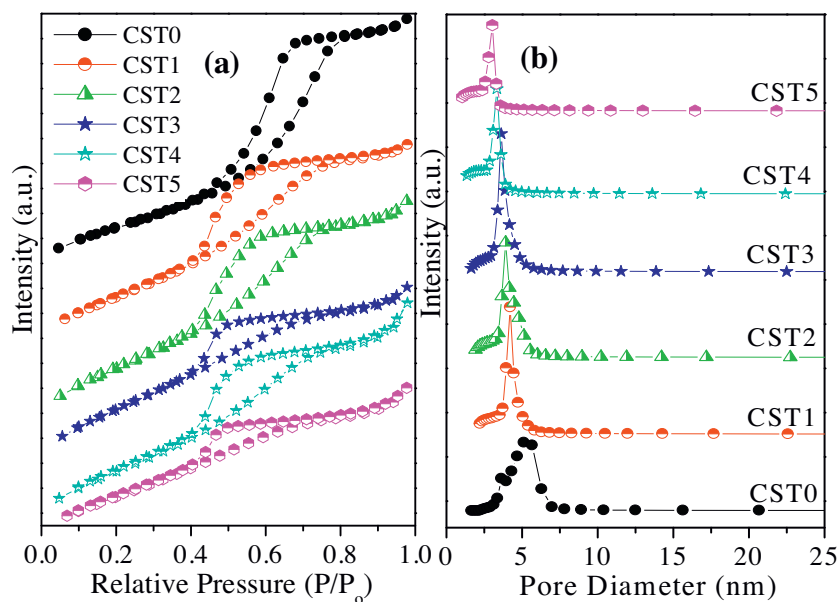


Fig. 3. N_2 adsorption-desorption isotherms (a) and pore size distribution curves (b) of different samples.

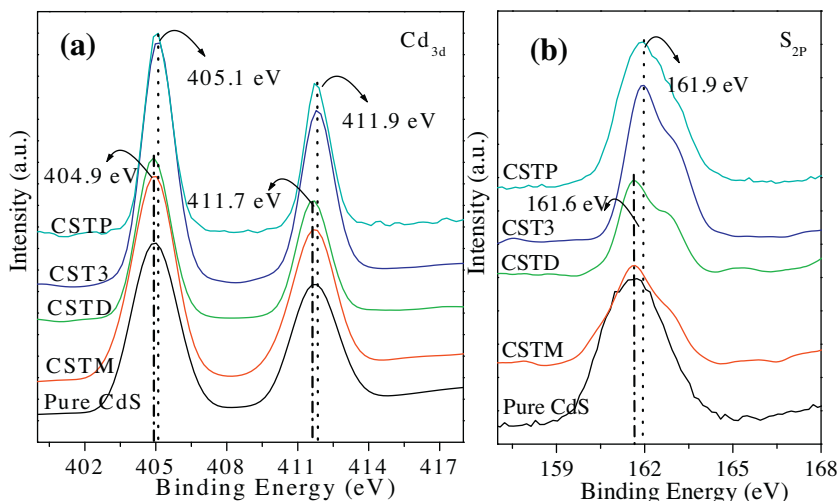


Fig. 4. The XPS spectra of different samples: Cd_{3d} of (a) and S_{2p} of (b).

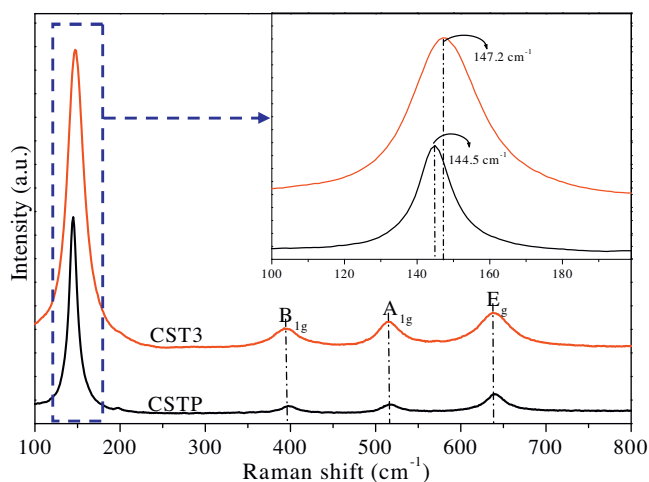


Fig. 5. Raman spectra of CST3 and CSTP; the inset shows the magnified Raman spectra in the range from 100 to 200 cm^{-1} .

clearly demonstrated that CST3 showed a positive shift of the principal peak by about 3.0 cm^{-1} in comparison with CSTP, corresponding to an increase in the number of surface oxygen vacancies, which further confirmed that the CST3 was comprised of TiO_2 crystal with exposed (001) facets while CSTP contained TiO_2 crystal with dominant (101) facets [10]. The (001) and (101) facets have different coordination numbers of Ti atom. In the (001) facet, each Ti atom is coordinated with 5 oxygen atoms, while in the (101) facet, each Ti coordinated is with either 5 or 6 oxygen atoms, with a probability of around 50–50%. Thus, the (001) facet displayed an increased number of oxygen vacancies in comparison with the (101) facet due to the lower coordination number of Ti with oxygen [10–14].

Fig. 6 demonstrates that all the CST3, CSTP, CSTD and CSTM samples generated photocurrent under visible light irradiation, and then rapidly decreased to zero when the light irradiation was turned off, which could be attributed to the photosensitizing effect of CdS (see Fig. 7) [17,18,27–29], taking into account that the pure TiO_2 couldn't be activated by visible lights with wavelength above 420 nm due to its big band gap (3.2 eV). With the same CdS load-

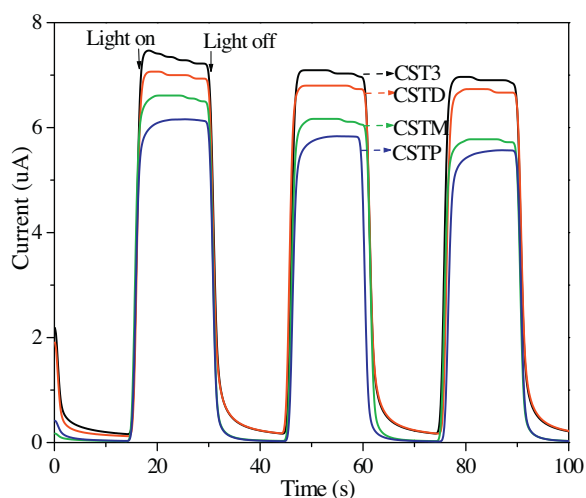


Fig. 6. Photocurrent responses of different samples.

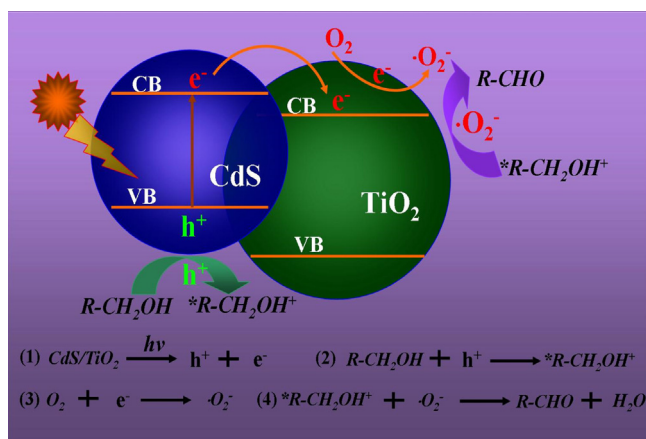


Fig. 7. The schematic illustration of the CdS photosensitizing effect, the electron transfer from CdS to TiO₂ via the heterojunction, and mechanism of photocatalytic selective oxidation of alcohol to aldehyde.

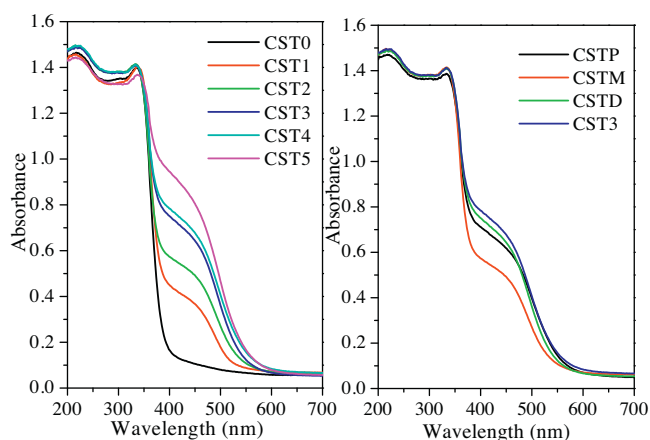


Fig. 8. UV-vis DRS spectra of different samples.

ings, the photocurrent intensity increased from CSTP, CSTM, CSTD to CST3 owing to the enhanced light-harvesting and/or the reduced photoelectron-hole recombination rate. As shown in Fig. 8, the UV-vis DRS spectra demonstrated that the absorbance for visible lights in CSTX samples increased with the increase of CdS loading, corresponding to the enhanced photosensitizing effect owing to the

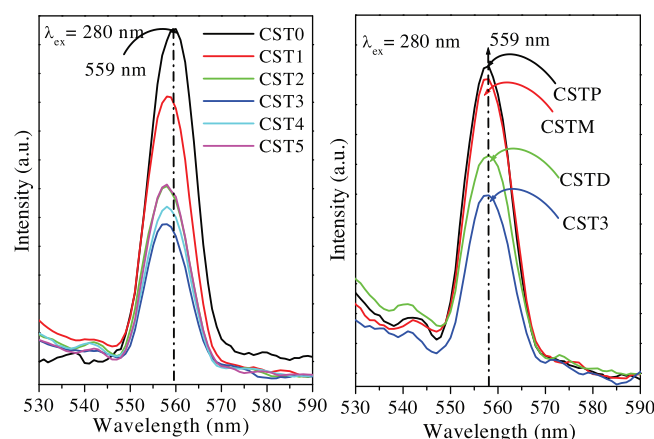


Fig. 9. PLS spectra of different samples.

increase in the number of CdS quantum dots. With the same CdS loadings, the absorbance for visible lights around 420 nm changed in the order of CSTM < CSTP < CSTD < CST3. Taking into account the similar size and thus, the similar number of CdS quantum dots in CSTP and CST3, the higher light-harvesting ability of CST3 was mainly ascribed to the exposed (001) facets, which enhanced the CdS-TiO₂ interaction and thus, promoted the photosensitizing effect from CdS. The CSTD exhibited poor light-harvesting ability due to the larger CdS particle size, which decreased the number of CdS nanoparticles and thus, reduced photosensitizing effect from CdS. This could also account for the weakest light-harvesting of CSTM, taking into account of the largest size of CdS particles in CSTM. Meanwhile, the PLS spectra in Fig. 9 reveals that the intensity of emission peak around 560 nm decreased with the increase of the CdS loading up to 3.5 wt% in CSTX samples, corresponding to the reduced recombination rate between photoelectrons and holes [19,20]. This could be attributed to the enhanced number of CdS-TiO₂ heterojunctions, which facilitated the transfer of photoelectrons from CdS to TiO₂ and thus, promoted the separation of photoelectrons from holes (see Fig. 7). Further increase in the CdS loading (>3.5 wt%) caused rapid photoelectron-hole recombination due to the abrupt increase of CdS nanoparticles, which initiated the rapid photoelectron-hole recombination within CdS semiconductor due to the narrow energy gap. The PLS spectra in Fig. 9 also demonstrates that photoelectron-hole recombination rate decreased from CSTP, CSTM to CST3, which could also be attributed to the remarkable increase in the size of CdS nanoparticles and the poor CdS-TiO₂ interaction in CSTP and CSTM. All the CSTD, CSTM and CST3 displayed lower photoelectron-hole recombination rate than CSTP owing to the exposed (001) facets, which generated more oxygen vacancies than the (101) facets. These oxygen vacancies could capture photoelectrons and thus, inhibited their recombination with holes [10,30].

3.2. Photocatalytic performances

The selective oxidation of alcohols to aldehydes is one of the most important functional group transformations used in fine chemicals [31–36]. Comparison with the traditional ways, the photocatalytic oxidation of alcohols displays advantages in saving energy and reducing environmental pollution since it could carry out under mild conditions without use of toxic oxidizing agents like chromates and manganese oxides [31–33]. Firstly, as a typical example, we explored the performance of CST3 in selective oxidation of benzyl alcohol to benzaldehyde under visible light irradiation. The HPLC-MS revealed that no significant side-products were detected, suggesting the absolute selectivity toward the tar-

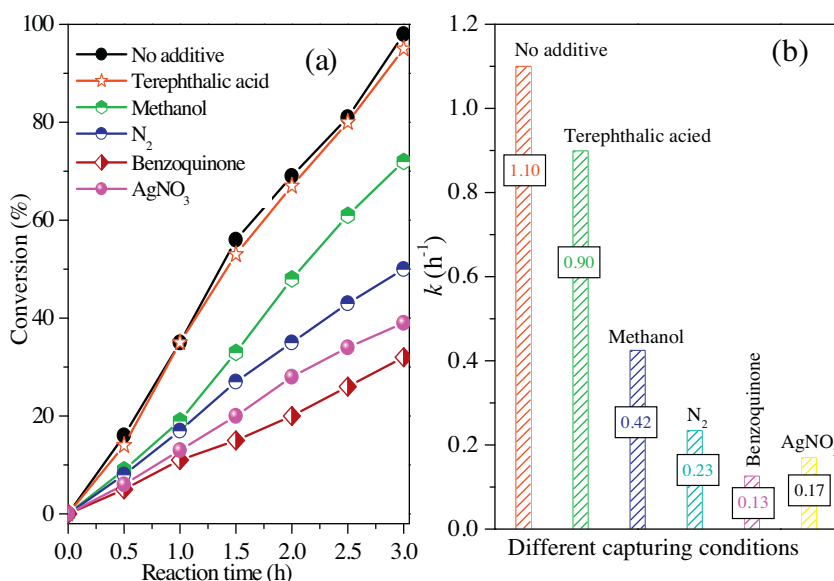


Fig. 10. Photocatalytic performances (a) and rate constant k (b) of CST3 for selective oxidation of benzyl alcohol in the presence of different capturers.

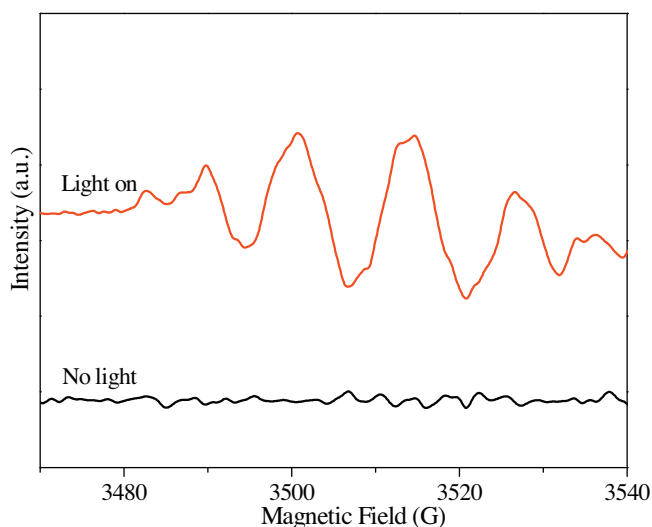


Fig. 11. ESR spectra of superoxide radical species trapped by DMPO over the CST3 sample dispersed in the benzotrifluoride solvent.

get product under the present conditions. As shown in Fig. 10a, no significant change in the reaction process was found when the terephthalic acid was added into the reaction system to capture $\bullet\text{OH}$ radicals [37]. However, abrupt decrease in the conversion of benzyl alcohol was observed by adding either methanol to capture photogenerated holes (h^+), or AgNO_3 to capture photoelectrons (e^-), or benzoquinone to capture $\bullet\text{O}_2^-$ radicals [38,39], or N_2 flow to eliminate dissolved O_2 . Meanwhile, the calculated rate constant k of benzyl alcohol conversion based on the pseudo-first-order (see Fig. 10b) further confirmed the above results. Electron spin resonance (ESR) spectra in Fig. 11 further confirmed the presence of $\bullet\text{O}_2^-$ radicals and the absence of $\bullet\text{OH}$ radicals in the present reaction system [35]. These results confirmed that, except for $\bullet\text{OH}$ radicals, all the photogenerated holes, photoelectrons and $\bullet\text{O}_2^-$ radicals were the active species for the present photocatalytic oxidation reaction, which could be briefly described in Fig. 7. Firstly, the CdS generated photoelectrons (e^-) and holes (h^+) under visible light irradiation, followed by transferring photoelectrons to TiO_2 through the CdS- TiO_2 heterojunctions. Then the photogenerated

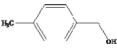
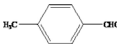
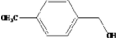
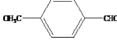
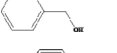

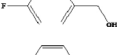
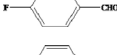
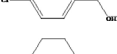
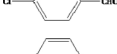
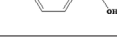
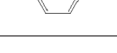
holes activated the absorbed benzyl alcohol to produce benzyl alcohol cation radicals and the photoelectrons activated the dissolved O_2 to form $\bullet\text{O}_2^-$ radicals. Finally, the $\bullet\text{O}_2^-$ radicals reacted with the benzyl alcohol cation radicals to produce benzaldehyde.

As shown in Table 1, CST0 displayed no significant activity since pure TiO_2 couldn't be activated by visible lights due to its big energy band gap (3.2 eV). With the increase of CdS loading from 0.85 to 3.5 wt%, the conversion of benzyl alcohol increased owing to the increase in both the surface area and the number of CdS quantum dots, which facilitated the diffusion and adsorption of reactant molecules, promoted the absorbance for visible lights, and also reduced the recombination rate between photoelectrons and holes. However, very high CdS loading (4.4 and 4.9 wt%) was harmful for the activity although the light-harvesting increased due to the decrease in surface area and the agglomeration of CdS quantum dots, which disfavored the diffusion and adsorption of reactant molecules, and also promoted the photoelectron-hole recombination. Thus, the CST3 was determined as the optimal photocatalyst in the present reaction, which also exhibited high activity and selectivity in photocatalytic oxidation of other benzylic alcohols to their corresponding aldehydes (see Table 2). It also displayed higher photocatalytic activity than either CSTD or CSTM owing to the smaller size and higher dispersion of CdS nanoparticles, corresponding to the higher surface area, the more CdS nanoparticles corresponding more CdS- TiO_2 heterojunctions as well as the stronger CdS- TiO_2 interaction, which facilitated diffusion and adsorption of reactant molecules, enhanced the photosensitizing effect and the absorbance for visible lights, and also reduced the photoelectron-hole recombination rate. Although the similar size and number of CdS nanoparticles, the CST3 still exhibited much higher activity than the CSTP owing to the exposed (001) facets. Firstly, in comparison with the (1 0 1) facets, the (001) facets displayed higher surface energy which favored the activation of reactant molecules. Meanwhile, the (001) facets also exhibited strong interaction with CdS nanoparticles, which might enhance the photosensitizing effect of CdS and also facilitated the photoelectron transfer from CdS to TiO_2 via heterojunctions. Furthermore, the (001) facets contained more oxygen vacancies than the (1 0 1) facets, which could capture photoelectrons and thus, inhibit their recombination with holes.

To determine the durability, the photocatalyst was allowed to centrifuge after each run of reactions, followed by washing thoroughly with distilled water and ethanol, respectively. Then, the

Table 2

Photocatalytic performances of CST3 in photocatalytic selective oxidation of benzylic alcohols.

Entry	Substrate	Product	Conversion (%)	Selectivity (%)	Yield (%)
1			98	98	96
2			100	99	99
3			95	100	95
4			83	100	83
5			89	100	89
6			91	100	91

photocatalyst was reused with fresh charge of reactants for the subsequent recycle of photocatalytic reaction under the identical reaction conditions. As shown in Table 1, CST3 could be used repetitively for at least 4 times without significant deactivation. However, the CSTD and CSTM displayed abrupt decrease in the conversion of benzyl alcohol in the fourth cycle. Since no significant change in either S_{BET} or D_p was observed, the decrease in the activity of CSTD and CSTM could be mainly attributed to the leaching of CdS, corresponding to the decrease of CdS-loading from 3.4 to 0.82 wt% for CSTD and from 3.5 to 0.75 wt% for CSTM as shown in Table 1. The CST3 displayed no significant CdS leaching possibly owing to the strong CdS-TiO₂ interaction against either CdS leaching or CdS corrosion, which could be confirmed by the good durability and little CdS leaching of CSTP.

4. Conclusions

In summary, this work developed a facile approach to prepare CdS quantum dots decorated TiO₂ mesocrystal with exposed (001) facets, which displayed high efficiencies in visible photocatalytic selective alcohol oxidations. The mesoporous structure with high surface area, the CdS quantum dots with enhanced photosensitization and heterojunction, the (001) facets with high surface energy and oxygen vacancy promoted the light-harvesting, photocatalyst activation, photoelectron-hole separation, and reactant molecule adsorption and activation. Meanwhile, the strong CdS-TiO₂ interaction could stabilized mesoporous structure and CdS, leading to the strong durability in photocatalysis.

Acknowledgments

This work is supported by NSFC (21237003, 21261140333, 21407106, 21522703 and 21503133), SICF (12230706000 and 13SG44), Natural Science Foundation of Shanghai City (15ZR1419100 and 14ZR1430800), Municipal Education of Shanghai (ZZGCD15031), The Program for Professor of Special Appointment (Eastern Scholar) at Shanghai Institutions of Higher Learning, Zhanchi Plan of Shanghai University of Engineering Science (nhrc-2015-12) and open topic fund of the Education Ministry Key Lab of Resource Chemistry of Shanghai ((2014) No. 18).

References

- [1] Z. Liu, X.D. Wen, X.L. Wu, Y.J. Gao, H.T. Chen, J. Zhu, P.K. Chu, J. Am. Chem. Soc. 131 (2009) 9405–9412.
- [2] R.Q. Song, A.W. Xu, M. Antonietti, H. Cölfen, Angew. Chem. Int. Ed. 48 (2009) 395–399.
- [3] R.Q. Song, H. Cölfen, Adv. Mater. 22 (2010) 1301–1330.
- [4] M. Niederberger, H. Cölfen, Phys. Chem. Chem. Phys. 8 (2006) 3271–3287.
- [5] J.F. Ye, W. Liu, J.G. Cai, S. Chen, X.W. Zhao, H.H. Zhou, L.M. Qi, J. Am. Chem. Soc. 133 (2011) 933–940.
- [6] L. Li, C.Y. Liu, CrystEngComm 12 (2010) 2073–2078.
- [7] P. Tartaj, J.M. Amarilla, Adv. Mater. 23 (2011) 4904–4907.
- [8] P. Tartaj, Chem. Commun. 47 (2011) 256–258.
- [9] Z.F. Bian, J. Zhu, J. Wen, F.L. Cao, Y.N. Huo, M.Q. Shen, H.X. Li, Y.F. Lu, Angew. Chem. Int. Ed. 50 (2011) 1105–1108.
- [10] J.G. Wang, Z.F. Bian, J. Zhu, H.X. Li, J. Mater. Chem. A 1 (2013) 1296–1302.
- [11] J. Pan, G. Liu, G.Q. Lu, H.M. Chen, Angew. Chem. Int. Ed. 50 (2011) 2133–2137.
- [12] Y.B. Zhao, W.H. Ma, Y. Li, H.W. Ji, C.C. Chen, H.Y. Zhu, J.C. Zhao, Angew. Chem. Int. Ed. 51 (2012) 3188–3192.
- [13] X.Q. Gong, A. Selloni, J. Phys. Chem. B 109 (2005) 19560–19562.
- [14] H.G. Yang, C.H. Sun, S.Z. Qiao, J. Zou, G. Liu, S.C. Smith, H.M. Cheng, G.Q. Lu, Nature 453 (2008) 638–641.
- [15] H.G. Yang, G. Liu, S.Z. Qiao, Y.G. Jin, S.C. Smith, J. Zou, H.M. Chen, G.Q. Lu, J. Am. Chem. Soc. 131 (2009) 4078–4083.
- [16] X.G. Han, Q. Kuang, M.S. Jin, Z.X. Xie, L.S. Zhang, J. Am. Chem. Soc. 131 (2009) 3152–3153.
- [17] W.T. Sun, Y. Yu, H.Y. Pan, X.F. Gao, Q. Chen, L.M. Peng, J. Am. Chem. Soc. 130 (2008) 1124–1125.
- [18] S. Banerjee, S.K. Mohapatra, P.P. Das, M. Misra, Chem. Mater. 20 (2008) 6784–6791.
- [19] G.S. Li, D.Q. Zhang, J.C. Yu, Environ. Sci. Technol. 43 (2009) 7079–7085.
- [20] Y.N. Huo, J. Zhu, H.X. Li, Appl. Catal. B 106 (2011) 69–75.
- [21] D.H. Chen, L. Cao, F.Z. Huang, P. Imperia, Y.B. Cheng, R.A. Caruso, J. Am. Chem. Soc. 132 (2010) 4438–4444.
- [22] J.G. Yu, L.F. Qi, M. Jaroniec, J. Phys. Chem. C 114 (2010) 13118–13125.
- [23] J. Zhu, S.H. Wang, J.G. Wang, D.Q. Zhang, H.X. Li, Appl. Catal. B 102 (2011) 120–125.
- [24] H.J. Huang, D.Z. Li, Q. Lin, W.Z. Zhang, Y. Shao, Y.B. Chen, M. Sun, X.Z. Fu, Environ. Sci. Technol. 43 (2009) 4164–4168.
- [25] J. Jiang, X. Zhang, P.B. Sun, L.Z. Zhang, J. Phys. Chem. C 115 (2011) 20555–20564.
- [26] S. Shenswi-Khalil, V. Uaarov, S. Fronton, I. Popov, Y. Sasson, J. Phys. Chem. C 116 (2012) 11004–11012.
- [27] J.T. Li, W.G. Hoffmann, H. Shen, C. Fabrega, T. Andreu, F.H. Ramirez, S. Mathur, J. Mater. Chem. 22 (2012) 20472–20476.
- [28] N. Zhang, Y.H. Yang, X.Y. Pan, M.Q. Yang, Y.J. Xu, J. Phys. Chem. C 116 (2012) 18023–18031.
- [29] S.Q. Liu, N. Zhang, Z.R. Tang, Y.J. Xu, ACS Appl. Mater. Interface 4 (2012) 6378–6385.
- [30] J.G. Wang, P. Zhang, X. Li, J. Zhu, H.X. Li, Appl. Catal. B 134–135 (2013) 198–204.
- [31] A. Tanaka, H. Kominami, Chem. Commun. 47 (2011) 10446–10448.
- [32] C. Aellig, C. Girard, I. Hermans, Angew. Chem. Int. Ed. 50 (2011) 12355–12360.
- [33] Q. Wang, M. Zhang, C.C. Chen, W.H. Ma, J.C. Zhao, Angew. Chem. Int. Ed. 49 (2010) 7976–7979.
- [34] Y. Uozumi, R. Nakao, Angew. Chem. Int. Ed. 42 (2003) 194–197.
- [35] Y.H. Zhang, N. Zhang, Z.R. Tang, Y.J. Xu, Chem. Sci. 3 (2012) 2812–2822.
- [36] Y.H. Zhang, Z.R. Tang, X.Z. Fu, Y.J. Xu, ACS Nano 5 (2011) 7426–7435.
- [37] S.B. Zhu, T.G. Xu, H.B. Fu, J.C. Zhao, Y.F. Zhu, Environ. Sci. Technol. 41 (2007) 6234–6239.
- [38] G.L. Huang, S.C. Zhang, T.G. Xu, Y.F. Zhu, Environ. Sci. Technol. 42 (2008) 8516–8521.
- [39] J.H. Kou, Z.S. Li, Y.P. Yuan, H.T. Zhang, Y. Wang, Z.G. Zou, Environ. Sci. Technol. 43 (2009) 2919–2924.